Int. J. Electrochem. Sci., 6 **(2011)** 4537 - 4552

International Journal of
ELECTROCHEMICAL
SCIENCE
www.electrochemsci.org

Palladium Particles Based Nano Films; Electrochemical Fabrication, Characterization and Applications

Soundappan Thiagarajan, Rong Fong Yang, Shen-Ming Chen[*]

Electroanalysis and Bioelectrochemistry Lab, Department of Chemical Engineering and Biotechnology, National Taipei University of Technology,No.1, Sec-3, Chung-Hsiao East Road, Taipei 106, Taiwan (R.O.C).
[*]E-mail: smchen78@ms15.hinet.net

Received: 25 August 2011 / *Accepted:* 22 September 2011 / *Published:* 1 October 2011

Palladium nanoparticles based composite electrodes have been fabricated using polyaniline (PA) and nordihydroguaiaretic acid (NDGA). Two types of nano palladium composite films were electrochemically fabricated using electroactive polymer PA and antioxidant NDGA. Both nanocomposite films were found to be electrochemically active and stable in various pH conditions. The surface morphologies of these two films were analyzed using AFM. PA-nano Pd film modified electrodes was employed for oxygen reduction reactions (ORR). Linear sweep voltammetry (LSV) was used to demonstrate the enhanced electrocatalytic activity of PA-nano Pd film modified GCE. Furthermore, chronoamperometric experiments were carried out to investigate the kinetic parameters of oxygen reduction reaction at this type of electrodes. In addition, the NDGA-nano Pd film modified electrodes were employed for the detection of As (III) in pH 7.0 PBS.

Keywords: Palladium, polyaniline, nordihydroguaiaretic acid, electrochemical deposition, nanocomposite film, oxygen reduction.

1. INTRODUCTION

Electrode modifications and the electrochemical fabrication of nanocomposite films at the electrode surface were widely studied [1-9]. Particularly, electroactive polymer and nanomaterials combined electrodes brought special attention for the detection various important chemical compounds. In noble metal nanoparticles, nano palladium keens a special interest because of its biocompatibility for the detection of various types of biological compounds [10]. On the other hand, polyaniline (Scheme-1), known as an electroactive polymer, has been utilized for the various types of electrode modifications. Polyaniline and palladium combined films were found to be electrochemically active and utilized for the various types of applications. For example, electrodeposition and

electrochemical behavior of palladium particles at polyaniline and polypyrrole films [11], palladium-containing polyaniline and polypyrrole micro particles [12], catalytic properties of palladium-containing electroactive polymers [13], electrocatalytic activity of platinum-polyaniline and palladium-polyaniline systems [14], nanosized metallic particles in polyaniline [15], electrochemistry of multilayer electrodes [16], electrocatalytic behavior of a palladium–polyaniline system [17], polyaniline films containing palladium micro particles [18], electrochemical and chemical interactions between polyaniline and palladium nanoparticles [19], graphite electrode modified with a polyaniline film containing electrodeposited palladium for the electrocatalytic oxidation of ascorbic acid [20], palladium electrodeposition on polyaniline films [21] and palladium on polyaniline modified carbon fiber paper for folic acid oxidation were reported [22].

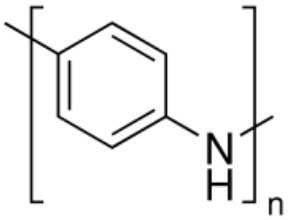

Scheme 1. Polyaniline

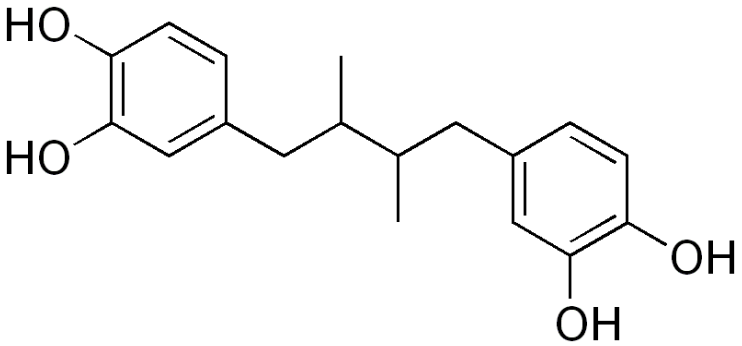

Scheme 2. Nordihydroguaiaretic acid (NDGA)

Next the 1, 4-Bis (3, 4-dihydroxyphenyl)-2, 3-dimethylbutane (nordihydroguaiaretic acid) known as NDGA, (Scheme 2) is natural product obtained from the creosote bush. NDGA has been utilized as antioxidant to preserve the foods and applied as anticancer agent [23]. NDGA also applied in electroanalytical applications. For example, NDGA/FAD hybrid film modified electrodes for NADH/NAD^+ redox reaction [24], electrochemical self-assembly of NDGA/nafion modified electrodes and their electrocatalytic properties for catecholamines and ascorbic acid [25], electrocatalytic properties of NDGA and spontaneous formation of an electroactive co-polymeric film derived from NDGA and 4,40-diaminobibenzyl [26], electrocatalytic thin films based on NDGA-functionalized polyaniline [27] and electrochemical conversion of poly-aniline into a redox polymer in the presence of NDGA [28] were successfully reported. Further the interaction of NDGA with

palladium nanoparticles has not reported yet. Therefore, we have focused to fabricate palladium nanoparticles combined NDGA film. In this report we have aimed to fabricate two types of palladium based films by electrochemical deposition process. Polyaniline (PA)-nano Pd and NDGA-nano Pd films were successfully fabricated on GCE and ITO electrodes. The electrochemical behaviors of the Polyaniline (PA)-nano Pd, NDGA-nano Pd films were examined in various buffer conditions. The surface nature of PA, NDGA, PA-nano Pd and NDGA-nano Pd films were thoroughly examined by using AFM technique. PA-nano Pd and the NDGA-nano Pd film modified GCEs were successfully employed for the oxygen reduction reaction (ORR) and detection of As (III) in pH 7.0 PBS solution.

2. MATERIALS AND METHODS

2.1. Reagents

Potassium tetra chloro palladate (II) was obtained from Strem chemicals (USA). Aniline (99.8 % pure) was purchased from Acros organics (Belgium). Nordihydroguaiaretic acid (97 % pure), was purchased from Sigma-Aldrich (USA). All other chemicals (Merck) used in this investigation were of analytical grade (99 %). Double distilled deionized water was used to prepare all the solutions. A phosphate buffer solution (PBS) of pH 7.0 was prepared using Na_2HPO_4 (0.05 M) and NaH_2PO_4 (0.05 M). Pure nitrogen was passed through all the experimental solutions.

2.2. Apparatus

Electrochemical measurements like cyclic voltammetry (CV), linear sweep voltammetry (LSV) was performed using CHI 410a potentiostats (CH Instruments, Austin, TX). A conventional three-electrode system was used throughout the experiments. The BAS glassy carbon electrodes (GCE) (φ = 0.3 cm in diameter) were in the form of disks sealed in a Teflon jacket having an exposed geometric surface area of 0.07 cm^2. The working electrode was a bare or PA-nano Pd (or) NDGA-nano Pd film modified GCE. Platinum wire auxiliary electrode and an Ag/AgCl (3 M KCl) reference electrode were used in the voltammetric measurements. All the potentials mentioned in this paper were referred to this reference electrode. The morphological characterization of the PA, NDGA, PA-nano Pd and NDGA-nano Pd film were studied by using AFM (Being Nano-Instruments CSPM-4000). Indium tin oxide (ITO) thin film coated glass electrode was used for AFM analysis.

2.3. Fabrication of PA-nano Pd and NDGA-nano Pd Film

Prior to electrode modification, the bare GCE was polished with the help of BAS polishing kit by using aqueous slurries of alumina powder (0.05 μm), rinsed and ultrasonicated in double distilled deionized water. The electrochemical polymerization process of aniline was obtained by immersing GCE in 0.5 M H_2SO_4 solution containing 0.05 M aniline monomer with a repetitive potential scan between 0 and 1 V (at the scan rate of 0.1 V s^{-1}) for three cycles (Inset of Fig. 1(A)). Further the polyaniline modified GCE was carefully washed with ultrapure water and immersed in 0.5 M H_2SO_4

solution containing 1×10^{-3} M potassium tetra chloro palladate (II), with a repetitive potential scan between 1.2 and -0.25 V (at the scan rate of 0.1 V s^{-1}) for three cycles (Fig. 1(A)).

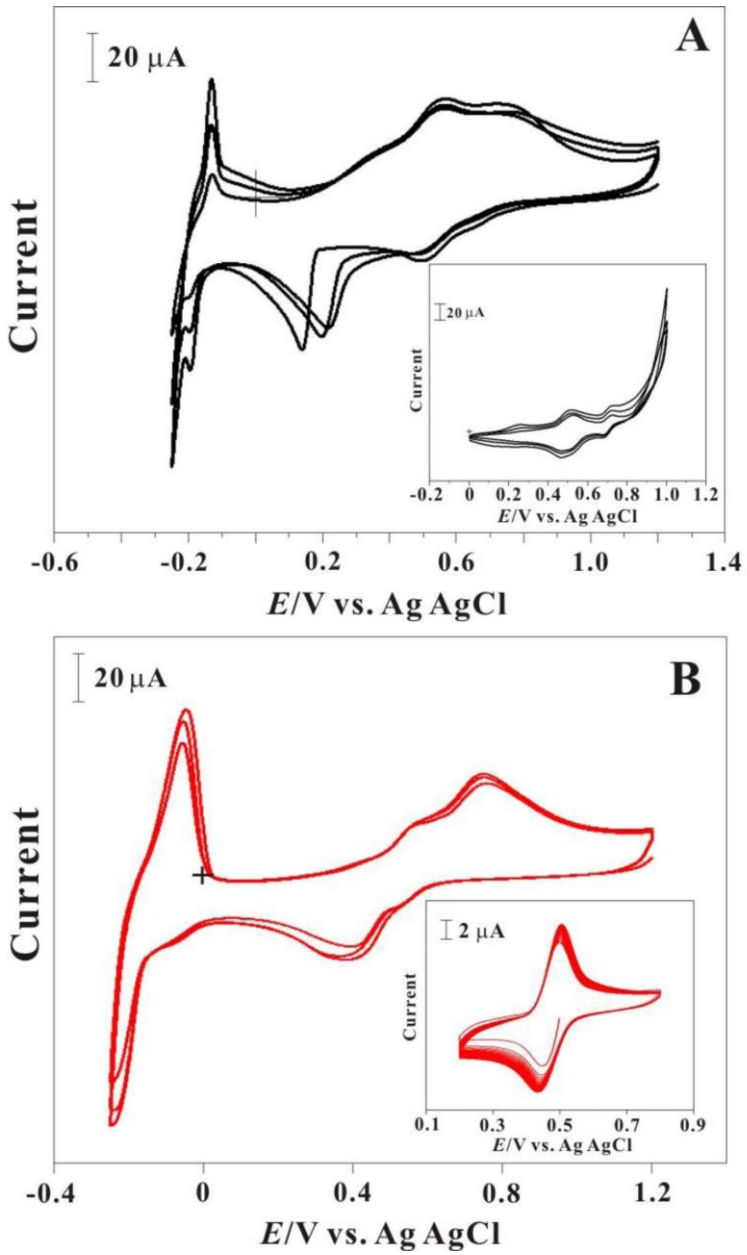

Figure 1. (**A**) CVs of Pd particles deposition process on PA modified GCE in 0.5 M H_2SO_4 containing 1×10^{-3} M potassium tetra chloro palladate (II), with a repetitive potential scan between 1.2 and -0.25 V (at 0.1 V s^{-1}) for three cycles. **Inset:** CVs of electrochemical synthesis process of PA on GCE from 0.5 M H_2SO_4 containing 0.05 M aniline monomer and the cycling potentials in the range of 0 – 1 V/s (at 0.1 V s^{-1}) for three cycles. **(B)** CVs of Pd particles deposition process on NDGA modified GCE in 0.5 M H_2SO_4 containing 1×10^{-3} M potassium tetra chloro palladate (II), with a repetitive potential scan between 1.2 and -0.25 V (at 0.1 V s^{-1}) for three cycles. **Inset:** CVs of electrochemical synthesis process of NDGA film on GCE from pH 1.5 H_2SO_4 containing 1 mM NDGA and the cycling potentials in the range of 0.2 – 0.8 V/s (at 0.1 V s^{-1}) for twenty cycles.

The another film NDGA was fabricated as follows; The electrochemical deposition process of NDGA was obtained by immersing GCE in pH 1.5 H_2SO_4 solution containing 1 mM NDGA with a repetitive potential scan starts at 0.5 V in initial and between 0.2 to 0.8 V (at the scan rate of 0.1 V s^{-1}) for twenty cycles (Inset of Fig. 1(B)). Further the NDGA film modified GCE was carefully washed with ultrapure water and immersed in 0.5 M H_2SO_4 solution containing 1×10^{-3} M potassium tetra chloro palladate (II), with a repetitive potential scan between 1.2 and -0.25 V (at the scan rate of 0.1 V s^{-1}) for three cycles (Fig. 1(B)). Afterwards, both the PA-nano Pd and NDGA-nano Pd films were rinsed with deionized water and placed in the electrochemical cell containing pH 7.0 PBS for different scan rate studies.

3. RESULTS AND DISCUSSION

3.1. Characterization of PA-nano Pd Film

As can be seen in the inset of Fig. 1 (A), the electrooxidation of aniline starts at 0.22 V in the first cycle renders the first layer of PA. For the continuous cycles the corresponding peaks growth indicates the growth of polymer film on the electrode surface. Further the voltammogram obtained for the electro synthesis of polyaniline shows three redox peaks at around 0.22, 0.5 and 0.7 V. This result clearly validates the presence of PA film on the GCE surface. Next, Fig. 1(A) shows the CVs of Pd nanoparticles deposition process on PA modified GCE surface. Here the voltammogram show the characteristic current features for Pd reduction (0.2 V), Pd oxide formation (0.72 V) hydrogen adsorption and desorption (-0.2 V) process. On scanning the potential in the negative direction, Pd particles is deposited on the electrode surface and when the potential reaches negative values, the peak at -0.2 V shows the reduction process of protons to hydrogen, which is adsorbed on the palladium surface.

This confirms that the hydrogen adsorption process simultaneously occur with the Pd particles deposition process. Next the scanning in the positive direction, peak at -0.18 V appears due to the oxidation of hydrogen atoms. Also in the positive direction, Pd particles deposited on the GCE surface are oxidized to Pd^{2+} and form a palladium oxide layer (0.72 V). Here the palladium oxide layer is not so obvious because of the presence of redox peaks of PA at the similar potentials. Furthermore, formed Pd oxides are reduced on the negative-going scans, leading back to Pd particles with hydrogen adsorption process. During the repetitive scan process, all the peaks were found growing which shows the Pd particles deposition on the electrode surface. Also the voltammetric peak currents growth with number of cycles (three) confirms the progressive increase in the metal particles distribution. Further at 0.3 to 0.7 V the presence of broad redox couples confirms the presence of electro synthesized PA on the GCE surface.

In the next step, the electrodeposited PA-nano Pd film has been examined for different scan rate studies (0.01 to 0.2 V/s) in pH 7.0 PBS which has been shown in Fig 2(A). Here the cathodic reduction peak currents of PA-nano Pd were linearly proportional to the scan rate in the range of 0.01 to 0.2 V s^{-1} as expected for a surface confined process. Also, in the higher scan rate studies a clear

decrease in the peak potentials separation between Pd and PA occurs and exhibits as a single redox peak (at around -0.2 and 0.2 V), respectively.

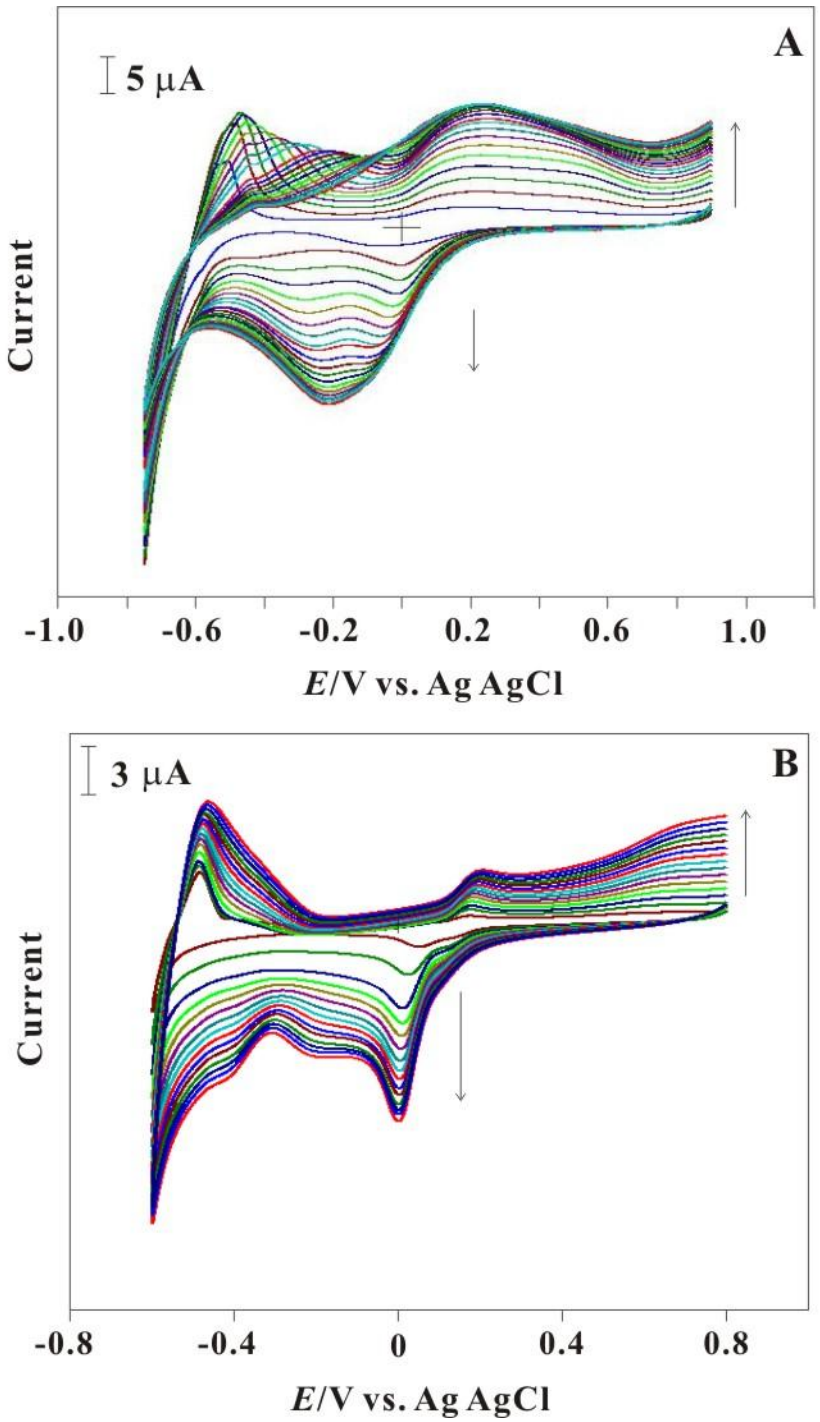

Figure 2. (A) Different scan rate studies of PA-nano Pd film modified GCE in pH 7.0 PBS solution (0.01, 0.02, 0.03, 0.04, 0.05, 0.06, 0.07, 0.08, 0.09, 0.1, 0.11, 0.12, 0.13, 0.14, 0.15, 0.16, 0.17, 0.18, 0.19 and 0.2 V s^{-1}). **(B)** Different scan rate studies of NDGA-nano Pd film modified GCE in pH 7.0 PBS solution (0.01, 0.02, 0.03, 0.04, 0.05, 0.06, 0.07, 0.08, 0.09, 0.1, 0.11, 0.12, 0.13, 0.14 and 0.15 V s^{-1}).

3.2. Characterizations of NDGA-nano Pd film

Inset of Fig. 1(B) shows the electrochemical deposition of NDGA starts at 0.5 V and the subsequent depositions of NDGA occur between 0.2 to 0.8 V for twenty cycles. Here, we can clearly see the growth of the NDGA single redox peak (the reduction and oxidation of NDGA occurs at 0.45 and 0.5 V). This result clearly depicts the electrochemical synthesis of NDGA film on the GCE surface. Next, the Fig 1(B) shows the CVs of Pd nanoparticles deposition process on NDGA film modified GCE.

Here the voltammogram show the characteristic current features for Pd reduction (0.4 V), Pd oxide formation (0.75 V), hydrogen adsorption and desorption (-0.24 and -0.04 V) process. On scanning the potential in the negative direction, Pd particles is deposited on the electrode surface and when the potential reaches negative values, the peak at -0.2 V shows the reduction process of protons to hydrogen, which is adsorbed on the palladium surface. This confirms that the hydrogen adsorption process simultaneously occur with the Pd particles deposition process. Next the scanning in the positive direction, peak at -0.04V appears due to the oxidation of hydrogen atoms. Also in the positive direction, Pd particles deposited on the GCE surface are oxidized to Pd^{2+} and form a palladium oxide layer (0.75 V).

Further the formed Pd oxides are reduced on the negative-going scans, leading back to Pd particles with hydrogen adsorption process. During the repetitive scan process, all the peaks were found growing which shows the Pd particles deposition on the electrode surface. Also the voltammetric peak currents growth (three cycles) confirms the palladium particles distribution process. In addition, a small redox couple at around 0.52 to 0.55 V represents the presence of electrosynthesized NDGA on the GCE surface. In the next step, the electrodeposited NDGA-nano Pd film has been examined for different scan rate studies in pH 7.0 PBS which has been shown in Fig 2(B). From the different scan rate studies, it shows that in lower scan rate the peak potential separation between NDGA and nano Pd was obvious one and proportionally decreasing and becomes as a single reduction peak in the higher scan rates, respectively.

3.3. AFM Studies

Atomic force microscopic analysis will provide more detailed information regarding the surface morphologies of the modified electrodes.

Table 1. AFM analysis of PA-nano Pd film

Parameters	PA film	PA-nano Pd film
Average Roughness (AR)	0.747 nm	5.44 nm
Root Mean Square Roughness (RMS)	0.949 nm	7.06 nm
Skewness (Sk)	-0.00421	0.32
Kurtosis (Ku)	2.95	3.61

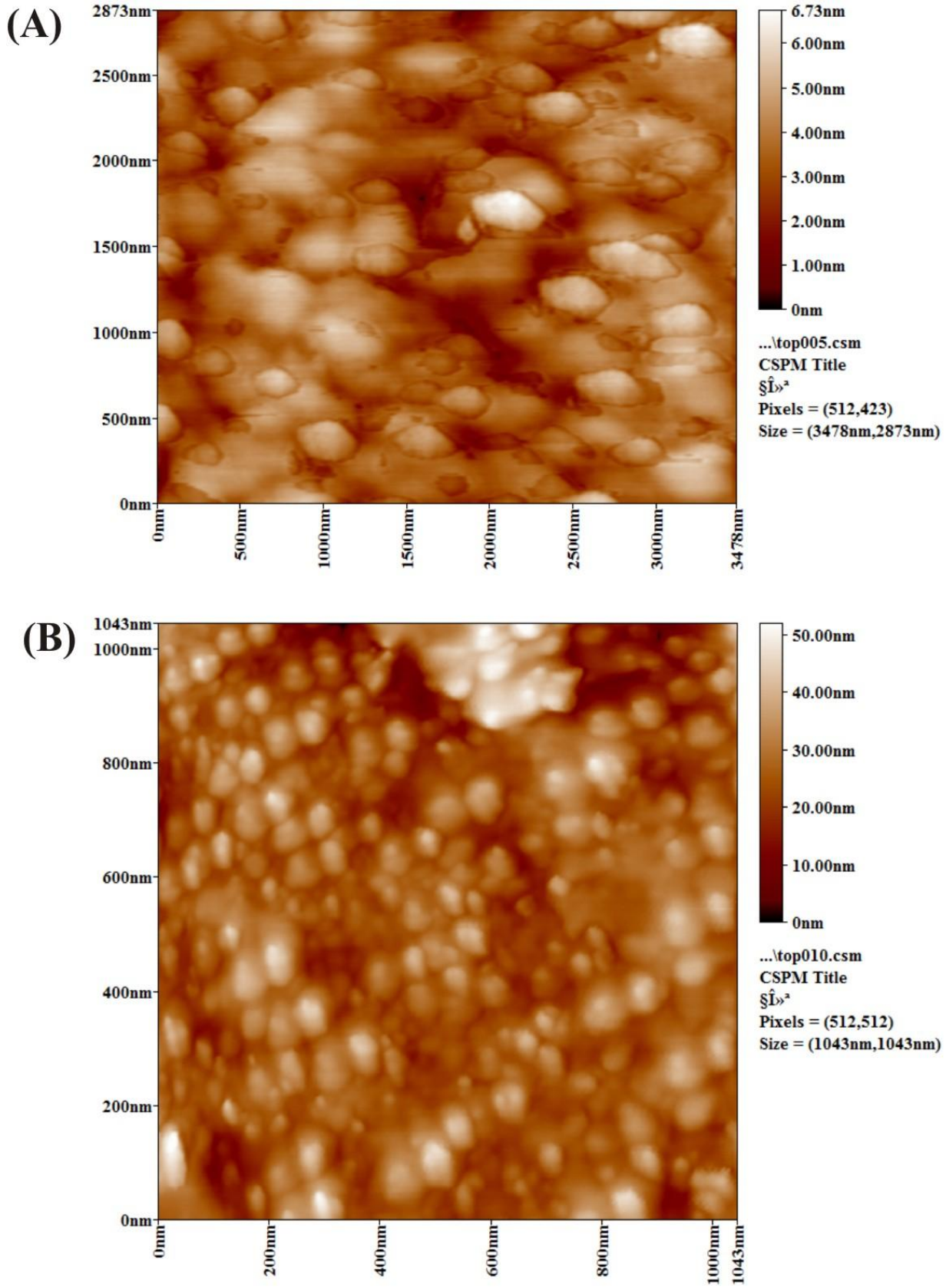

Figure 3. **(A)** AFM two dimensional view of PA film, **(B)** PA-nano Pd film.

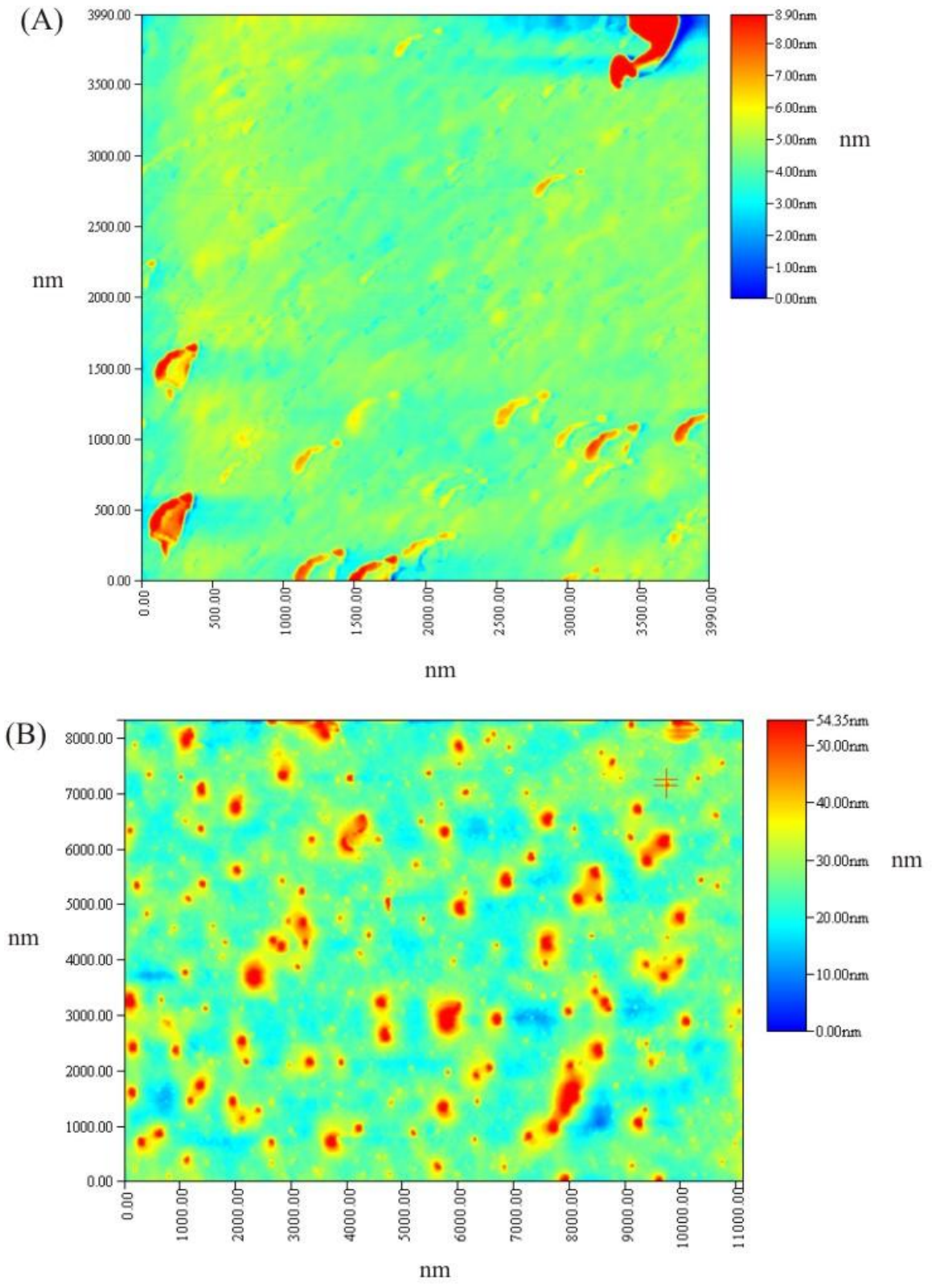

Figure 4. (A) AFM two dimensional view (multicolor) of NDGA film, **(B)** NDGA-nano Pd film.

Fig. 3(A) and (B) show the two dimensional analysis of PA and PA-nano Pd film modified ITO. Tapping mode has been employed for the analysis. The scanning area was limited to 3478 × 2873

nm for PA and 1043 × 1043 nm for PA-nano Pd film modified ITO. From the Fig. 3(A) we can clearly notice the existence of PA film on the ITO surface. Here the PA film electrodeposited as closely packed with beads like structure, respectively. Also, the polymer film possesses porous structures on its surface. Here the average roughness (AR) for the PA film was found as 0.747 nm. Fig. 3(B) shows the PA-nano Pd film modified ITO. From this two dimensional image it can be seen that the nano Pd particles were embedded into the porous nature of the PA film.

From this bi-layer film deposition process analysis, it was found that the embedded Pd nanoparticles will act as active centers for the electrocatalytic reactions. Generally, the sample roughness corresponds to the surface nature and particle size distribution of the film.

Here the average roughness (AR) value (table-1) was obtained from image topography of PA-nano Pd film. These values are averages calculated from several images acquired in different regions of the respective sample. Generally, low AR value resembles the uniform deposition and surface nature of the film [29]. Here the AR values obtained from the AFM analysis shows that the nano particles were unevenly deposited on the PA film surface.

In addition, the bare ITO surface exhibits a very smooth morphology, with the RMS roughness being smaller than 0.25 nm. However, the increase of the RMS roughness of PA-nano Pd film may be due to the increase of density and size of Pd nanoparticles on the PA film surface. Next in AFM parameter analysis, the surface skewness (Ssk) depicts the asymmetric nature of the height distribution in the sample. Also the negative values of Ssk for the PA film indicate the surface-porous nature. Here the nano Pd particles were deposited on the porous nature of the PA film.

Thus, positive value (0.32) was obtained for the PA-nano Pd film. Further the surface kurtosis (Ku) value illustrates the sharpness of the surface height distribution. For PA-nano Pd film, the Ku value was found as 3.61, which refers that the PA-nano Pd film surface has almost quantized height values. Further the grain size analysis reports that the total no of nano Pd particles deposited on the PA film surface was found as 248. Furthermore, the average height of the film was 8.9 nm. Also, the average diameters of the nano Pd particles from these calculations were found as 46.9 nm. Finally, this AFM analysis results illustrate the surface nature of the PA-nano Pd film and confirm the deposition of nano Pd particles on the PA film surface.

Table. 2 AFM analysis of NDGA-nano Pd film

Parameters	NDGA film	NDGA-nano Pd film
Average Roughness (AR)	0.433 nm	4.55 nm
Root Mean Square Roughness (RMS)	0.731 nm	6.42 nm
Skewness (Sk)	1.9	1.56
Kurtosis (Ku)	16.5	6.66

Next Fig. 4(A) and (B) shows the two dimensional multi color view of NDGA film and NDGA-nano Pd film electrochemically deposited onto the ITO surface. Here the tapping mode was employed for all type of AFM analysis. In Fig. 4(A), the fluorescent yellow color region shows the

electrochemically deposited NDGA film on ITO surface. Here the NDGA film was deposited as a very thin layer onto the electrode surface. Next in the Fig. 4(B) the red colored region shows the presence of palladium nanoparticles.

Furthermore, the remaining green color region shows the NDGA film surface. From the AFM analysis, it was clearly proved that the palladium nanoparticles were deposited onto the NDGA film surface. From this bi-layer film deposition process analysis, it was found that the embedded Pd nanoparticles will act as active centers for the electrocatalytic reactions. Further the sample roughness which corresponds to the surface nature of the film has been examined for two types of films and the results were given in Table-2. These values are averages calculated from several images acquired in different regions of the respective samples. The NDGA-nano Pd films have higher roughness comparing with the NDGA film on electrode surface. This is because of the presence of nano Pd on the NDGA film surface. Also the higher roughness value shows that the film possesses the higher electrocatalytic activity.

3.4. pH studies of PA-nano Pd and NDGA-nano Pd film

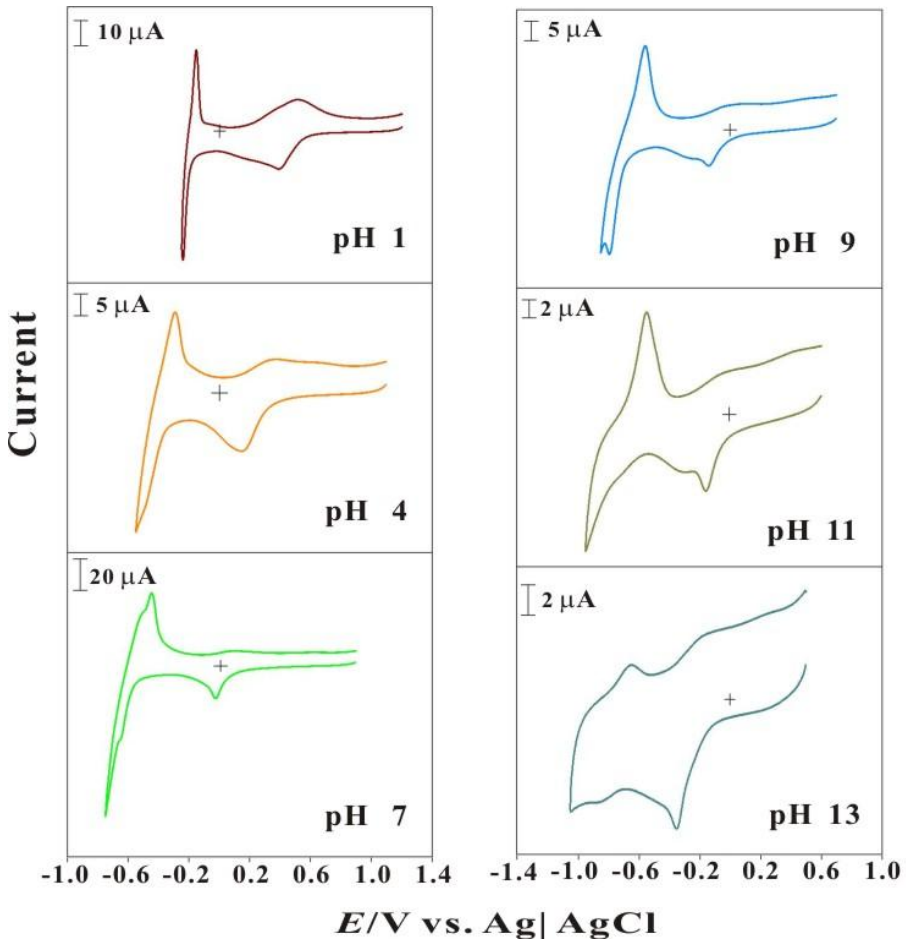

Figure 5. PA-nano Pd film in different pH solutions.

Fig. 5 shows the CVs of PA-nano Pd film in various pH solutions. Here the values of E_{pa} and E_{pc} for PA-nano Pd film depend on the pH of buffer solutions. Further increase in pH leads to a negative shift in potentials for both the reduction and oxidation peaks of PA and Pd. Here, except pH 13, in all pHs the PA-nano Pd film clearly exhibits the hydrogen adsorption and desorption process. Further in pH 9 and 11 buffer solutions we can see both the reduction peaks of nano Pd and PA. However, in the other buffer solutions we can observe the integrated reduction peaks of PA and Pd. Here I_{pc} and I_{pa} of PA-nano Pd show a maximum current response at pH 1 and 4 buffer solutions. In pH 7 to 13 buffer solutions the peak currents of PA-nano Pd film decreases substantially.

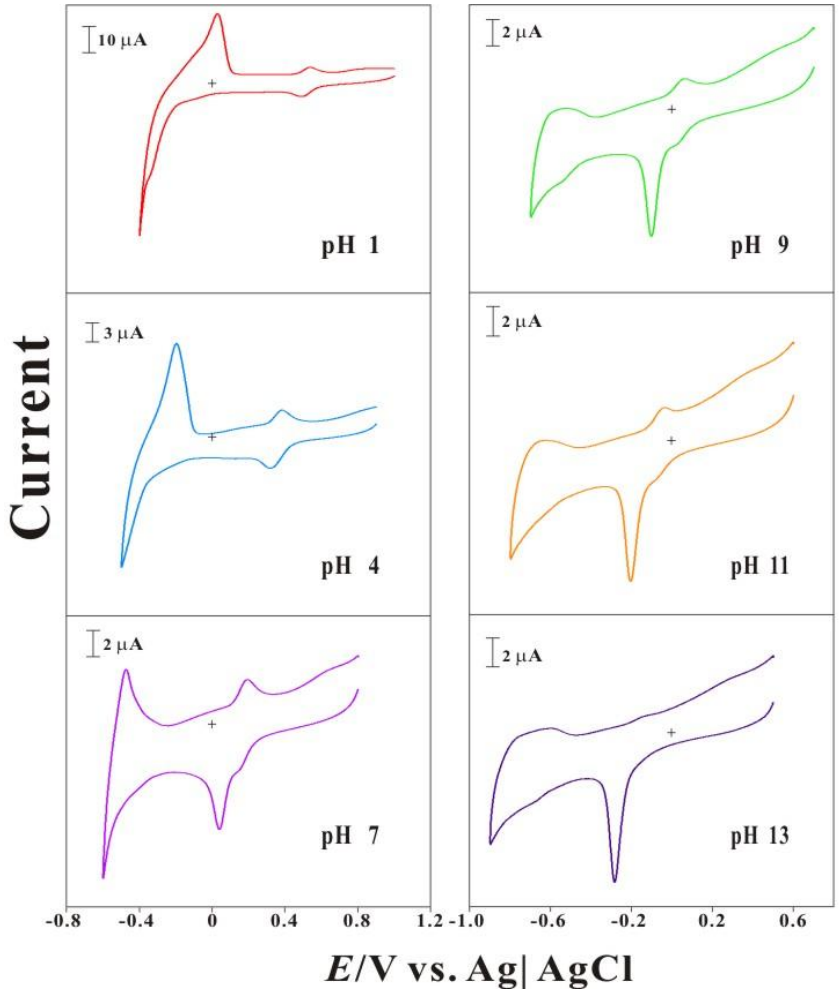

Figure 6. NDGA-nano Pd film in different pH solutions.

In the next step NDGA-nano Pd film modified GCE has been examined in the various pH solutions (Fig. 6). In pH 1 and 4 buffers solutions it obviously exhibits only the redox peak of NDGA and the hydrogen adsorption desorption process. This is because the reduction of Pd occurs in the same potential of NDGA. Next in pH 7 PBS solution, we can clearly see the reduction peak separation between NDGA and nano Pd. This indicates that in this pH both the NDGA and nano Pd were active. Also in pH 9, we can easily distinguish the reduction and oxidation peaks of NDGA and Pd in separate manner. In pH 11 it shows a slightly diminished peak of NDGA. However in this pH the bi-layer film

shows an obvious reduction peak of nano Pd. Finally, in pH 13 its shows only the reduction and oxidation peak of nano Pd. In this pH NDGA is not electrochemically active. From these illustrations it concludes that in basic pH condition only nano Pd is active. Thus we have selected the physiological pH 7.0 PBS for the electro catalysis reactions in which both the NDGA and nano Pd films were active.

3.5. Oxygen reduction reaction at PA-nano Pd film modified GCE

Electrocatalytic activity of the PA-nano Pd film for oxygen reduction reaction (ORR) was ascertained by recording linear sweep voltammograms (LSV) for the O_2 saturated pH 7.0 PBS solution. Here the voltammetric result clearly demonstrates the excellent electro activity of PA-nano Pd film for ORR in comparing with the unmodified bare GCE. Fig. 7 shows the LSV responses of the PA-nano Pd film in O_2 saturated solutions. Reduction peak at -0.4 V was observed for the PA-nano Pd film for ORR during the cathodic scan of potentials (Fig. 7 (a-g)). Comparatively, there is no any reduction wave was noticed for ORR at the unmodified bare GC electrode (Fig. 1 line (a')). Thus, an enhanced electrocatalytic activity was noticed for PA-nano Pd film over the unmodified GC electrode with a gradual increase in the peak current for the ORR at around -0.4 V. This shows that the PA-nano Pd film effectively suits for the ORRs. Also, the obtained result is comparable with previous literature reports [30, 31]. Further PA-nano Pd film modified GCE was employed for the series of chronoamperometric studies. Fig. 8 shows the chronoamperograms of PA-nano Pd film were obtained by purging O_2 in pH 7.0 with different time intervals ((a) 0, (b) 30, (c) 90, (d) 150 (e) 360 and (f) 600s). Here the net current response of PA-nano Pd film for O_2 reduction were obtained (inset of Fig. 8) and the dependence of net current (I) was plotted vs. the time ($t^{1/2}/s^{-1/2}$) [32].

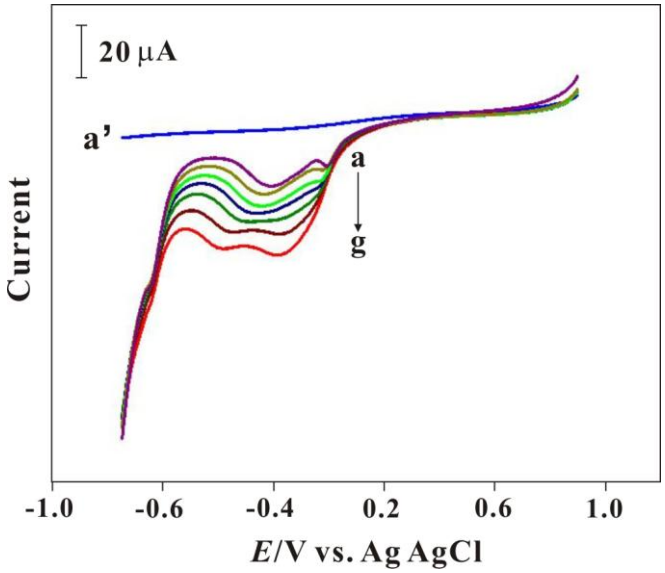

Figure 7. Linear sweep voltammograms of PA-nano Pd film on GCE for oxygen purging in pH 7.0 PBS with various time intervals (a-g; 0, 60, 120, 180, 240, 300,360 and 420s (a') bare GCE = 420s).

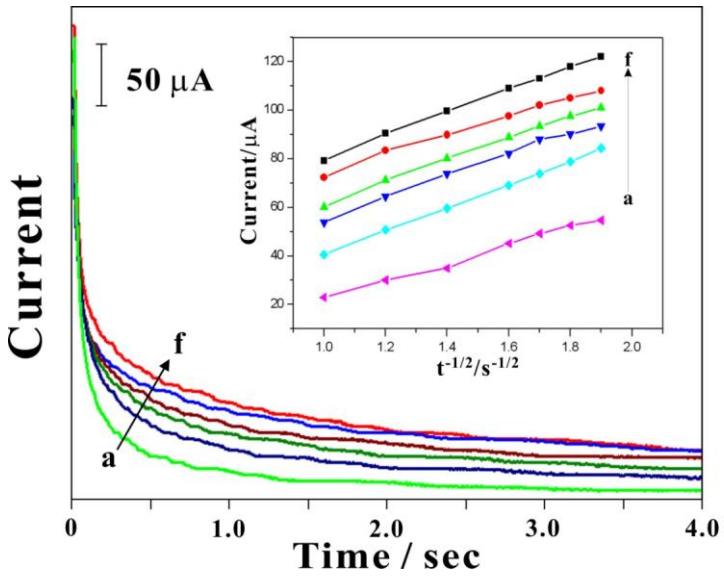

Figure 8. Chronoamperometric responses of PA-nano Pd film in pH 7.0 for oxygen purging in various time intervals. The curves (a)–(f) correspond to (a) 0, (b) 30, (c) 90, (d) 150 (e) 360 and (f) 600s of oxygen purging. Inset shows the plot of I vs. $t^{-1/2}/s^{-1/2}$ obtained from the chronoamperograms.

Further the diffusion coefficient could be estimated from the slopes of dependencies of the above plot using the Cottrell equation;

$$I = nFAD^{1/2} C_o/\pi^{1/2}t^{1/2}$$

Finally, from these results it was ascertained that the PA-nano Pd film effectively exhibits for oxygen reduction reactions.

3.6. Electrochemical detection of As (III) at NDGA-nano Pd film modified GCE

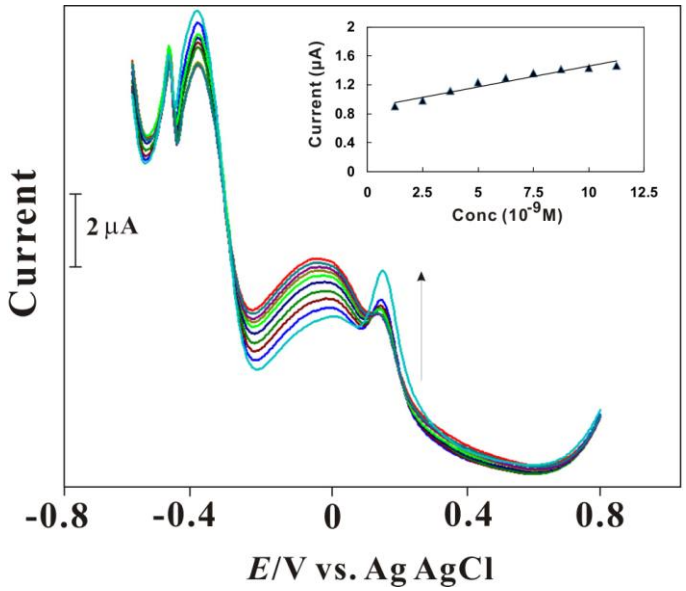

Figure 9. DPVs of NDGA-nano Pd film for As (III) detection in pH 7.0 PBS The As(III) concentrations were in the linear range of: 0, 1.2, 3.7, 5, 6.2, 7.5, 8.7, 10 and 11.2 × 10^{-9} M.

The fine performance of NDGA-nano Pd film modified GCE toward the detection of As (III) makes it attractive for the fabrication of arsenic sensors. Fig. 9 shows the typical DPV response of NDGA-nano Pd film modified GCE for the successive additions of As (III) in the range of 1.2 to 11.2 $\times 10^{-9}$ M. From Fig. 9, it can be seen that the peak current increases linearly at around -0. 05 V for the increasing concentrations of As (III). For the continuous additions of As (III), the corresponding peaks current were clearly increasing. This shows that the NDGA-nano Pd film clearly detects the As (III). Here the detection signals may not obvious because the nanomolar concentrations of As (III). Further the inset in Fig. 9 shows the anodic peak currents vs. concentration plot for As (III) detection. From the calibration plot, the linear regression equation for As (III) detection was found as $y = 0.0576x + 0.8813$, with a correlation coefficient of $R^2 = 0.941$. Finally, the above results validate the electrocatalytic detection of As (III) in nano molar concentrations at NDGA-nano Pd film modified GCE.

4. CONCLUSION

In conclusion, we have reported a detailed procedure for the electrochemical fabrication of PA-nano Pd and NDGA-nano Pd films on different electrodes like GCE and ITO. The surface morphological analysis such like AFM studies showed that the PA-nano Pd and NDGA-nano Pd films were found as bi-layer films on the electrode surface. Both bi-layer films show their own interesting electrochemical properties in the various buffer solutions. PA-nano Pd film successfully employed for the oxygen reduction reaction (ORR) and NDGA-nano Pd film modified GCE shows the detection signals for As (III). Furthermore, this type of films could be employed for the various types of electrocatalytic applications.

ACKNOWLEDGMENT
This work was supported by grants from National Science Council (NSC) of Taiwan (ROC).

References

1. C. Degrand, L.L. Miller, *J. Am. Chem. Soc.*, 102 (1980) 5728.
2. P. Shakkthivel, S.-M. Chen, *Biosens. Bioelectron.*, 22 (2007) 1680.
3. S. Thiagarajan, S.-M. Chen, *Talanta* 74 (2007) 212.
4. S. Thiagarajan, T.-H. Tsai, S.-M. Chen, *Biosens. Bioelectron.*, 24 (2009) 2712.
5. Y. Umasankar, S. Thiagarajan, S.-M. Chen, *Sensors* 8 (2008) 7191.
6. T.-H. Tsai, S. Thiagarajan, S.-M. Chen, *Electroanal.*, 22 (2010) 680.
7. S. Thiagarajan, S.-M. Chen, *J. Solid. State Electrochem.*, 13 (2009) 445.
8. T.-H. Tsai, S. Thiagarajan, S.-M. Chen, *J. Agr. Food. Chem.*, 58 (2010) 4537.
9. C.-Y. Cheng, S. Thiagarajan, S.-M. Chen, *Int. J. Electrochem. Sci.*, 6 (2011) 1331.
10. S. Thiagarajan, R.-F. Yang, S.-M. Chen, *Bioelectrochem.*, 75 (2009) 163.
11. A. Leone, W. Marino, B.R. Scharifker, *J. Electrochem. Soc.*, 139 (1992) 438.
12. S. W. Huang, K. G. Neoh, E. T. Kang, H. S. Han, K. L. Tan, *J. Mater. Chem.*, 8 (1998) 1743.

13. S.W. Huang, K.G. Neoh, C.W. Shih, D.S. Lim, E.T. Kang, H.S. Han K.T. Tan, *Synthetic met*., 96 (1998) 117.
14. B. I. Podlovchenko, Yu. M. Maksimov, T. D. Gladysheva, E. A. Kolyadko, Russ. *J. Electrochem*., 36 (2000) 731.
15. J. Wang, K. G. Neoh, E. T. Kang, *J. Colloid. Interf. Sci*., 239 (2001) 78.
16. A. Frydrychewicz, A. Czerwinski, K. Jackowsk, *Synthetic. Met*., 121 (2001) 1401.
17. Y. M. Maksimov, E. A. Kolyadko, A. V. Shishlova, and B. I. Podlovchenko, Russ. *J. Electrochem*., 37 (2001) 777.
18. A. Mourato, S. M. Wong, H. Siegenthaler, L. M. Abrantes, *J. Solid. State. Electrochem*., 10 (2006) 140.
19. J.-E. Park, S.-G.Park, A. Koukitu, O. Hatozaki, N. Oyama, *Synthetic. Met*., 141 (2004) 265.
20. L.G. Shaidarova, A.V. Gedmina, I.A. Chelnokova, G. K. Budnikov, *J. Anal. Chem*., 61(2006) 601.
21. A. Mourato, J.P. Correia, H. Siegenthaler, L.M. Abrantes, *Electrochim. Acta* 53 (2007) 664.
22. R.B. Moghaddam, P.G. Pickup, *Electrochim Acta* 56 (2011) 7666.
23. N. Fujimoto, R. Kohta, S. Kitamura, H. Honda, *Life Sci*., 74 (2004) 1417.
24. S.-M. Chen, M.-I. Liu, *Electrochim. Acta* 51 (2006) 4744.
25. S.-M. Chen, M.-I. Liu, *J. Electroanal. Chem*., 579 (2005) 153.
26. G. Milczarek, *Electrochem. Commun*., 9 (2007) 1761.
27. G. Milczarek, *React. Funct. Polym*., 68 (2008) 1542.
28. G. Milczarek, *J. Electroanal. Chem*., 626 (2009) 143.
29. S. Thiagarajan, T.-H. Tsai, S.-M. Chen, *Int. J. Electrochem. Sci.*, 6 (2011) 2235.
30. K. Ding, *Int. J. Electrochem. Sci.*, 5 (2010) 668.
31. K.-Q. Ding, *Int. J. Electrochem. Sci.*, 5 (2010) 72.
32. H.-W. Cheng, S. Thiagarajan, S.-M. Chen, *Int. J. Electrochem. Sci.*, 6 (2011) 4150.